Experimental Validation of a Combined Electromagnetic and Thermal FDTD Model of a Microwave Heating Process

Lizhuang Ma, Dominique-Lynda Paul, Nick Pothecary,
Chris Railton, John Bows, Lawrence Barratt, Jim Mullin, and David Simons

Abstract—**Microwave cooking, tempering, and pasteurizing of foods involves several complex and interacting physical phenomena. Although such processes are widely used, the interactions between the food product, packaging, and the microwave oven itself are particularly complicated, are not well understood, and applicable simulation tools are lacking. In this contribution we describe a combined finite difference time domain model for the electromagnetic and the heat transfer processes which include temperature dependence of the electrical and thermal properties of the food product. This model is validated by comparison to experiment.**

I. Introduction

MICROWAVE COOKING, thawing, tempering, and pasteurizing of foods involves several complex and interacting physical phenomena. Although such processes are widely used, the interactions between the food product, packaging and the microwave oven itself are particularly complicated and are not well understood and applicable simulation tools are lacking. The type of oven and the shape, size, geometry, and temperature of the product all have substantial effects on the heating characteristics. By contrast with conventional heating methods, microwave heating can be more rapid due to the fact that the heating takes place, to a greater or lesser extent, throughout the interior of the food. This volumetric heat delivery leads to a much higher rate of heating than conduction limited, conventional heating methods, and microwave heating times are typically much shorter. However, the corollary of any volumetric heating method is that if uneven heating occurs, "hot" or "cold spots" can occur which do not have sufficient time to equilibrate by the end of heating. For food products, this can deleteriously effect product quality. Much effort, both in industry and in academia, is being applied to the design of oven geometries which will provide efficient, rapid, and uniform heating to the product. The existence of a computer model which is capable of predicting the performance of an arbitrary oven geometry with realistic products would complement and reduce the empiricism of the experimental work being undertaken. Perhaps due to the complexity of the problem, such models are lacking. Much recently published work e.g., [1]–[4] is limited to relatively simple situations which either do not include coupling between the electromagnetic and thermal processes, or are restricted to two-dimensional approximations and so are a long way from a realistic domestic or industrial system. In [5] the coupled problem has been solved for a homogeneous workload using a form of the method of lines [6]. Unfortunately, details of the numerical scheme are not given and there is no experimental comparison. In this contribution we analyze the behavior of a domestic microwave oven containing a representative workload by means of a mathematical model, based on finite difference time domain methods, developed at Bristol and by means of experimental measurements carried out at Unilever Research and we show that good agreement has been obtained. The efficiency of the computer algorithm is such that all the modelling work was carried out on the widely available HP730 workstation without excessive run times.

Manuscript received September 21, 1994; revised August 1, 1995. This work was supported in part by the UK Science and Engineering Research Council.

L. Ma, D.-L. Paul, N. Pothecary, and C. Railton are with the Center for Communications Research, Faculty of Engineering, University of Bristol, Bristol, BS8 1TR, England.

J. Bows, L. Barratt, J. Mullin, and D. Simons are with the Unilever Research Colworth Laboratory, Colworth House, Sharnbrook, Bedford, MK44 1LQ, England.

IEEE Log Number 9414852.

II. The Experimental Arrangement

In order to carry out the validation, the Panasonic Genius model NN6857 microwave oven containing a somewhat idealized but not unrepresentative workload was chosen. The dimensions of this oven and the load are shown in Figs. 1 and 2. Also shown here is the mesh used in the modeling described later. Although the oven normally operates with a turntable, this was disabled throughout the experiments to exaggerate the temperature differences in the work load and simplify the assumptions. The load used during the experiment and simulation was a phantom food gel possessing similar properties to meat [7]. In order to maintain the shape of the gels, PTFE containers were used. Prior to the experiments, the gels (and the containers) were sliced through the horizontal plane of symmetry, in order to ease the task of thermal imaging, and chilled to 5°C. PVC film was used to keep the two halves separate. The composition of the phantom food load is given in Table I and is a modified form of the TX151 gelling agent, which is detailed in [7].

The dielectric properties of the phantom food loads were measured, using the HP85070A dielectric probe kit which is based on an open coaxial probe and an HP8510 automatic

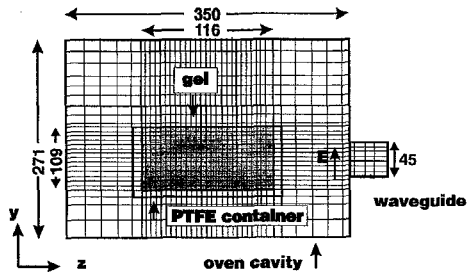

Fig. 1. Geometry of the Panasonic Genius NN6857 microwave oven, (side view).

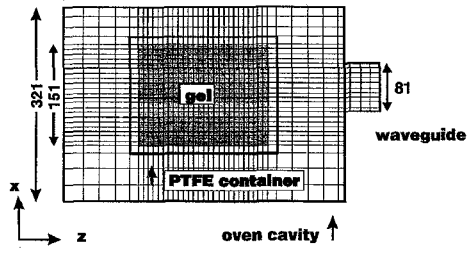

Fig. 2. Geometry of the Panasonic Genius NN6857 microwave oven, (plan view).

network analyzer [8] and the thermal data used was taken from the literature [7]. The gel data used in the simulations is presented in Table II. For temperatures greater than 48° C, it was assumed that the permittivity remained constant.

For the PTFE the properties were considered to be independent of temperature and were taken from [9]. They are shown in Table III.

The gels were stored overnight at a temperature of 5° C, this being the initial temperature used throughout the simulations. A ambient temperature of 30°C was assumed together with a convective heat transfer coefficient of 10 Wm^{-2} K^{-1}, corresponding to a flow of air of approximately 0.5 ms^{-1} across the surface via the action of the oven fan.

Two different configurations of the workload were examined. In the first case, the phantom was placed so that its longer side was parallel to the feed, the slab being positioned such that the planes of horizontal and vertical symmetry of the load coincided with those of the feed. In the second case the load is displaced by 30 mm towards the rear of the oven.

In each case the oven was run for a period of 180 seconds after which the two halves of the slab were separated and thermal images were taken, using an Agema 870 camera, of the face of each half. The technique is similar to that used by Ohlsson and Risman in their study of microwave heating of cylinders and spheres [10], and for microwave cooking [11].

III. Overview of the Mathematical Model

Because of the complexity of the geometry of the structure and the fact that the material properties change as a function of temperature, and therefore as a function of time, the most appropriate mathematical method was considered to be the finite difference time domain technique. Two separate algorithms were used, the first being an enhanced version of the well known Yee algorithm [12] to solve the electromagnetic problem and the second being an explicit finite difference scheme to solve the heat transfer equations. The meshes for each algorithm were arranged such that a temperature node for the thermal algorithm was placed at the center of each unit cell of the electromagnetic mesh. This allowed the coupling between the two models to be conveniently calculated as detailed below. Because of the very different time steps which must be used for the two algorithms, O(ps) for the electromagnetics and O(s) for the thermal, the combined algorithm is implemented as follows. First the electromagnetic algorithm is run using the initial values of the material properties and with a sinusoidal excitation at the working frequency of 2.45 GHz. In order to avoid large transients which would delay the establishment of a steady state, the amplitude of the sinusoid is allowed to build up to its working level over a single cycle. When the fields have reached a steady state, typically after 4 or 5 cycles and determined by monitoring the total calculated dissipated power in the workload, the dissipated power at each cell in the domain is calculated from the rms field values and the electrical properties of the material. The thermal algorithm is then run using the dissipated power as input in order to calculate the rise in temperature at the center of each cell. The updated temperature information is used, in turn, to calculate the new material parameters. Although not necessary in the simulation described here, it would also be possible to simulate movement in the workload at this point. This would be appropriate for an industrial system in which

TABLE I
Composition of the Phantom Food Load

Percentage by weight	Component
25.00	Low density polyethylene
8.45	TX151 Polymer
66.55	De-ionised water

TABLE II
Properties of the Phantom Food Load in SI Units

Temperature	Dielectric constant $\varepsilon'/\varepsilon_0$	Dielectric Loss $\varepsilon''/\varepsilon_0$	Density $Kg\ m^{-3}$	Specific Heat $J\ Kg^{-1}\ K^{-1}$	Thermal Conductivity $J\ K^{-1}\ m^{-1}\ s^{-1}$
12.3	52	20	1000	3600	0.55
25.0	43	14.5	1000	3600	0.55
34.7	36	11.5	1000	3600	0.55
39.5	36	11.3	1000	3600	0.55
45.5	28.4	7.2	1000	3600	0.55
48.0	22.4	7.0	1000	3600	0.55

TABLE III
Properties of the PTFE Container in SI Units

Thermal Conductivity ($J\ K^{-1}\ m^{-1}\ s^{-1}$)	0.29
Density ($Kg\ m^{-3}$)	1375
Specific Heat ($J\ Kg^{-1}\ K^{-1}$)	1250
Dielectric Constant, $\varepsilon'/\varepsilon_0$	2.2
Dielectric Loss, $\varepsilon''/\varepsilon_0$	0.00032

TABLE IV
UNIT CELLS IN THE x DIRECTION

Unit cell	size(mm)
1-4	12
5-6	10
7-8	6
9-22	3.5
23-46	3.375
47-60	3.5
61-62	5.5
63-68	8 5

TABLE V
UNIT CELLS IN THE y DIRECTION

unit cell	size(mm)
1-10	10.25
11-12	7.5
13-14	5
15-24	3.5
25-40	3.75
41-50	3.5
51-52	6.75

product was passed through a heating tunnel on a conveyor belt. The above procedure is then repeated until the required heating time has been simulated. After the initial pass through this loop, the time taken for the electromagnetic algorithm to reach steady state is usually just one cycle since the field perturbation as a result of the change of temperature is small. Since the field perturbation due to the change in material properties with temperature will be small this is not expected to cause stability problems. No numerical instability was detected on any of the results obtained.

IV. THE FINITE DIFFERENCE MESH

The problem space was contained within a computational domain whose dimensions are 321 mm × 271 mm × 390 mm.

A non-uniform mesh consisting of 88 × 68 × 92 unit cells was then defined. Each unit cell takes the form of a Yee cell with the addition of an extra temperature node placed at its center. The sizes of the unit cells used are given in Tables IV–VI.

The gel occupied a cuboid from nodes 13–56 in the x direction, 19–46 in the y direction and 25–70 in the z direction.

TABLE VI
UNIT CELLS IN THE z DIRECTION

unit cell	size(mm)
1-4	7
5-8	3
9-10	3
11-12	5
13-16	8
17-18	7.5
19-20	5
21-42	3.5
43-52	3.4
53-74	3.5
75-76	5
77-78	7.5
79-84	10

The PTFE container was represented by a layer 2 nodes thick on the five surfaces of the workload.

V. THE POWER DISSIPATION DISTRIBUTION

The power dissipation distribution $P(x, y, z)$ was calculated with the basic equation

$$\boldsymbol{P} = (\omega\varepsilon_0\varepsilon'' + \sigma)\overline{E^2} \tag{1}$$

where $\overline{E}$ is the rms value of the E field, ε'' is the imaginary part of the complex permittivity and σ is the conductivity of the material. The thermal algorithm requires, as input, the power dissipated per unit volume at the center of the unit cell, i.e., at the position of the temperature node. In order to calculate this we need to know the rms E field at that point. Assuming the standard FDTD approximation of a linear variation of field versus distance and the fact that the nodes for the different E field components are offset from the origin of each cell, we use linear interpolation for the unit cell i, j, k as in (2) as shown at the bottom of the next page, where the rms value of E_x may either be calculated using (3) where the sum is updated at each FDTD iteration and reset to zero at the end of each cycle or by looking for the maximum value of the E field during each period and multiplying this by $\sqrt{2}$. Similar results were obtained whichever method was used

$$\overline{E_x} = \frac{\sqrt{2}\left|\sum_{n=0}^{N} E_x(n\delta t)\ \exp(j\omega n\delta t)\right|}{N} \tag{3}$$

δt is the FDTD time step and $N\delta t$ is the period of the sine wave used for excitation. Similar expressions are used for E_y and E_z.

The heat generation term in a specific unit cell is then given by the specific dissipation times the volume of the cell as shown in equation

$$Q' = \boldsymbol{P}\ \delta x\ \delta y\ \delta z. \tag{4}$$

The value of Q' is passed to the heat algorithm. In addition, by summing over all unit cells, we may calculate the total power dissipated in the workload.

VI. Calculating the Temperature Rise

The temperature rise is calculated using the heat conduction equation [13] given below

$$\frac{\partial T}{\partial t} = \alpha \nabla^2 T + \frac{Q'}{\rho c} \tag{5}$$

where T is the temperature, α is the thermal diffusivity, Q' is the heat generation term, ρ is the mass density and c is the specific heat. Alternatively, we can use $\alpha = \kappa/c\rho$ where κ is the thermal conductivity. All values are in SI units.

At the material surfaces, convective boundary conditions are used such that

$$q = hA(T_s - T_{\text{air}}) \tag{6}$$

where q is the heat transfer rate, h is the convection heat transfer coefficient, A is the surface area, T_s is the surface temperature of the workload and T_{air} is the temperature of the surrounding air.

Away from the surface we implement (5) in the following explicit finite difference form [14]

$$\begin{aligned} T^{n+1} = {} & F_o(T^n(i-1,j,k) + T^n(i+1,j,k) \\ & + T^n(i,j-1,k) + T^n(i,j+1,k) \\ & + T^n(i,j,k-1) + T^n(i,j,k+1)) \\ & + (1 - 6F_o)T^n(i,j,k) + \frac{Q'\delta t'}{\rho c} \end{aligned} \tag{7}$$

where $F_o = \alpha \delta t'/\delta x^2$, the superscript n refers to the time step and the indices i, j, k refer to the node position, i.e., $T^n(i,j,k) = T((i+1/2)\delta x, (j+1/2)\delta y, (k+1/2)\delta z, n\delta t')$ and $\delta t'$ is the thermal algorithm time step.

If there is a convective surface, (7) must be modified by replacing the conductive heat transfer rate by the convective heat transfer rate, q. For example if there is an interface between workload and air at $x = (i+1)\delta x$ we replace $(T^n(i+1,j,k) - T^n(i,j,k))\kappa\delta$ x with $(T_{\text{air}} - T^n(i,j,k))h\delta x^2$ from (6) yielding (8)

$$\begin{aligned} T^{n+1} = {} & F_o(2T^n(i-1,j,k) + T^n(i,j-1,k) \\ & + T^n(i,j+1,k) + T^n(i,j,k-1) \\ & + T^n(i,j,k+1)) + (1 - 6F_o - F_o(B_i - 1)) \\ & \cdot T^n(i,j,k) - F_o B_i T_{\text{air}} + \frac{Q'\delta t'}{\rho c} \end{aligned} \tag{8}$$

where $B_i = h\delta x/\kappa$.

For numerical stability we ensure that

$$\delta t' < \frac{\delta x^2}{6\alpha(1 + B_i)}. \tag{9}$$

VII. Updating the Material Parameters

Having used the thermal algorithm to update the temperatures at the centers of each unit cell, we need to update the electrical parameters of the material at each cell in accordance with Table II. In this case it is the temperature at the E field nodes of the cell which should determine the value of permittivity and conductivity to use and, therefore, we use the linear interpolations given in (10)–(12), as shown at the bottom of the next page, where $K_x(i,j,k)$ is the temperature which we use to calculate ε_x for the unit cell i, j, k and $K(i,j,k)$ is the temperature at the center of the cell i, j, k.

VIII. Specifying the Excitation

Energy is supplied to the cavity of the oven by means of the dominant TE10 mode of the rectangular waveguide. In the simulation, a plane within the waveguide is excited by equivalent electric and magnetic currents having the spatial distribution corresponding to this mode and with an amplitude which corresponds to an incident wave of the required power. In practice this is achieved by adding the appropriate values to the E_y and H_x nodes in the excitation plane. Energy which is reflected back due to a mismatch between the impedance of the waveguide and that of the loaded cavity passes through the excitation plane, which appears transparent, and is absorbed by the absorbing boundary.

In order to apply, as closely as possible, the same power in the simulation as was actually supplied during the experiment, the amount of power coupled into and dissipated within the gel was evaluated from the temperature rise measured using the thermal imaging. By solving for a normalized E field and making some assumptions concerning the amount of power reflected, we can calculate the field amplitude required to yield that power input to the gel via the approach outlined by Barratt [15]. The power dissipated in the experimental workload was estimated to be approximately 600 Watts based on a measurement performed in accordance with IEC 705.

Unlike many applications of the FDTD technique, it was found that sinusoidal excitation was more efficient than pulse excitation for this type of problem. In some cases it has been shown that, even if results are required at only one frequency, it may be more efficient to use a pulse rather than a sinusoid. In the work described here, however, that was not found to be the case.

$$\begin{aligned} \overline{E^2}(i,j,k) = {} & \left(\frac{\overline{E_x}(i,j,k) + \overline{E_x}(i,j+1,k) + \overline{E_x}(i,j,k+1) + \overline{E_x}(i,j+1,k+1)}{4}\right)^2 \\ & + \left(\frac{\overline{E_y}(i,j,k) + \overline{E_y}(i+1,j,k) + \overline{E_y}(i,j,k+1) + \overline{E_y}(i+1,j,k+1)}{4}\right)^2 \\ & + \left(\frac{\overline{E_z}(i,j,k) + \overline{E_z}(i+1,j,k) + \overline{E_z}(i,j+1,k) + \overline{E_z}(i+1,j+1,k)}{4}\right)^2 \end{aligned} \tag{2}$$

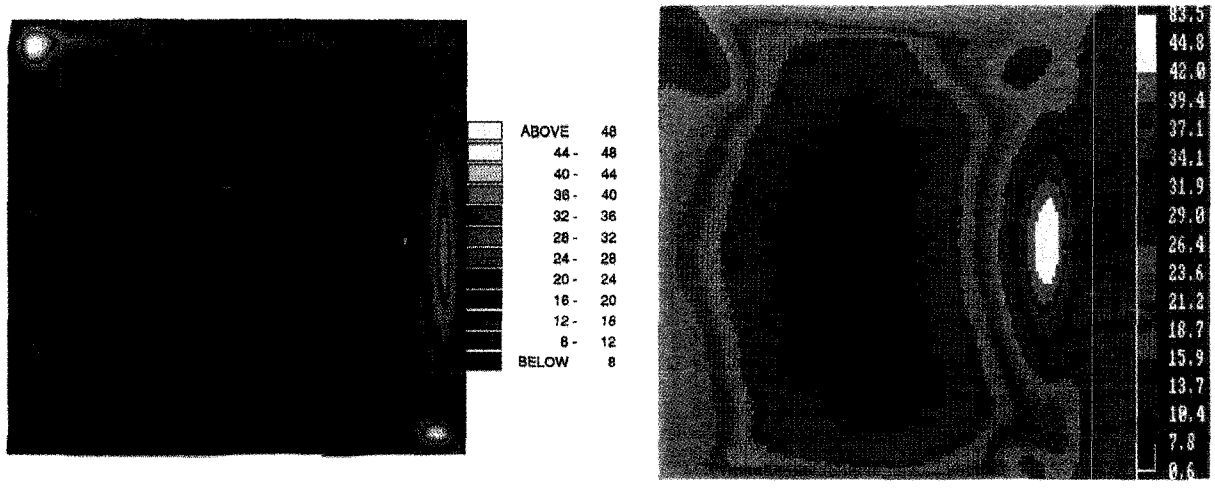

(a) (b)

Fig. 3. Calculated and measured temperature distribution, 180 seconds. (Case 1—Horizontal plane)

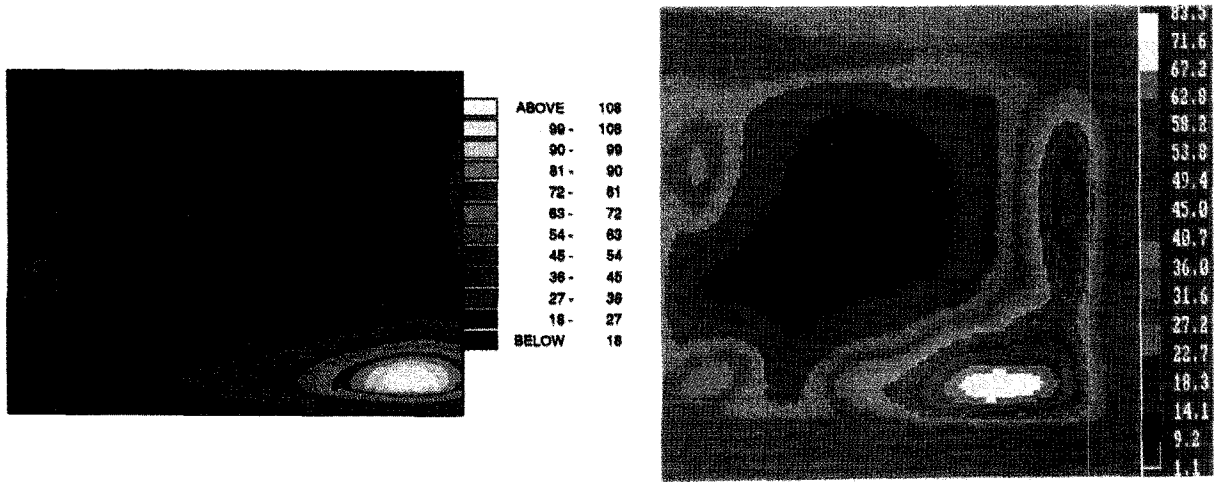

(a) (b)

Fig. 4. Calculated and measured temperature distribution, 180 seconds. (Case 1—Vertical plane)

IX. Treatment of Material Boundaries

It is well known that where there is an interface between materials of different electrical properties, both the field and the temperature will vary rapidly. This is especially true if we have a corner or a sharp edge. Care must be taken in these cases or the temperature rise near edges and boundaries will be overestimated. Using (2), which assumes linear variation of the field, under these conditions will give a result which is higher than reality and consequently an overestimate to the temperature rise. Instead we may calculate the field at the temperature node by making use of our knowledge of the asymptotic field behavior to provide a better estimate.

X. Comparison of Theoretical and Experimental Results

The measured and calculated results for the two cases under investigation are shown in Figs. 3–6. It can be seen that in each case the main features of the heating pattern have been correctly predicted by the model. In particular the hot spots along the center of the front face of the load and at the corners.

$$K_x(i,j,k) = \frac{K(i,j,k) + K(i,j-1,k) + K(i,j,k-1) + K(i,j-1,k-1)}{4} \tag{10}$$

$$K_y(i,j,k) = \frac{K(i,j,k) + K(i-1,j,k) + K(i,j,k-1) + K(i-1,j,k-1)}{4} \tag{11}$$

$$K_z(i,j,k) = \frac{K(i,j,k) + K(i,j-1,k) + K(i-1,j,k) + K(i-1,j-1,k)}{4} \tag{12}$$

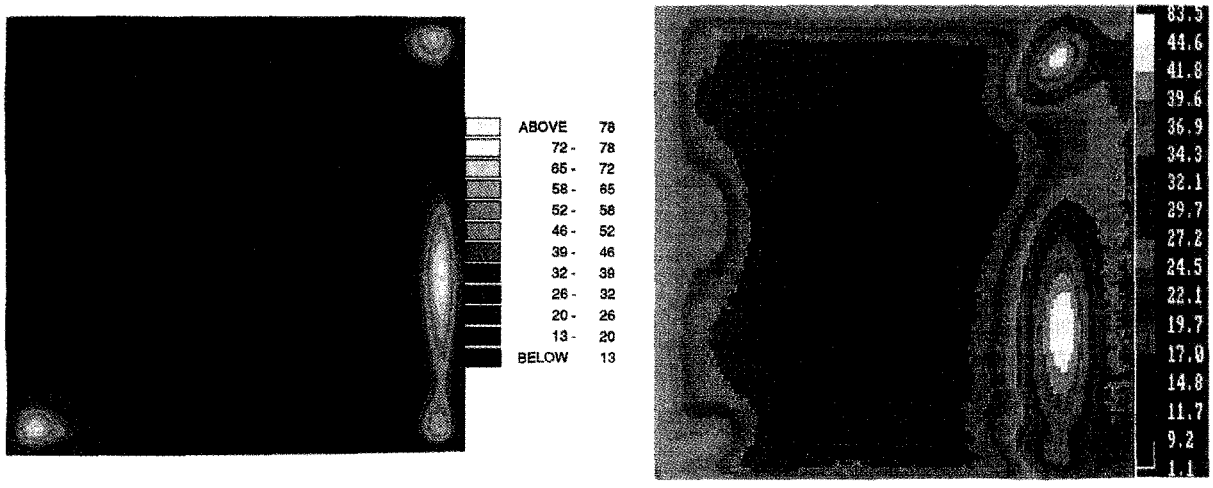

(a) (b)

Fig. 5. Calculated and measured temperature distribution, 180 seconds. (Case 2–Horizontal plane)

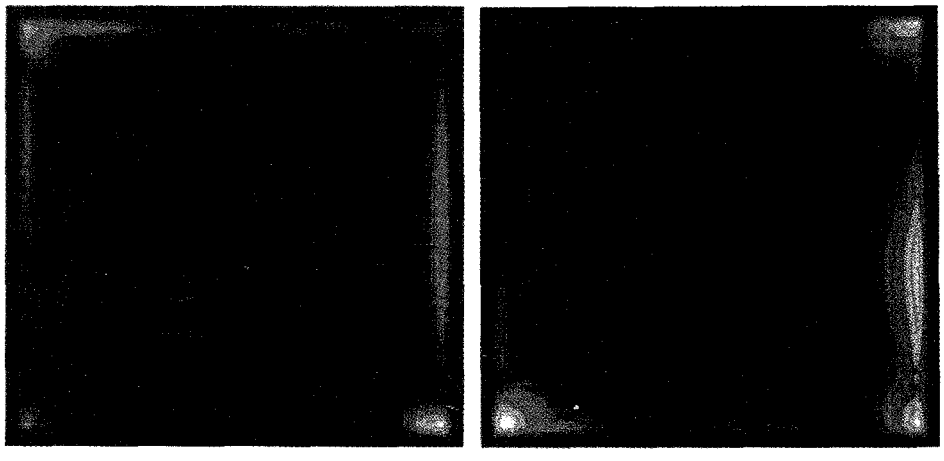

(a) (b)

Fig. 6. Simulated power dissipation. (Cases 1 and 2—Horizontal plane)

Due to the asymmetry of the oven, the position of the hot spot on the face is not in the center of the workload even when the load was placed symmetrically with respect to the waveguide feed, i.e., the energy is being applied to the system from the right of the figure and vertically symmetrical with respect to it. This indicates that the model is capable of handling subtle changes in cavity dimensions. The corner effects have been somewhat overestimated by the model and this may be for a number of reasons. It is partly caused by incomplete treatment of the rapid variation of fields in these areas. In addition some cooling will have taken place in the experiment before the thermal image was taken. This effect is estimated to cause an error of the order of 3–5°C. Another possible difference between the model and the experimental data is in the thermal imaging. There could, for example, be disturbance to the local temperature distribution when the clingfilm between the two halves was removed. In addition, air trapped between the two halves as the load was assembled may have led to gel movement on opening the box up.

The measured and calculated temperature distribution in the vertical plane is shown in Fig. 4. Here we see that most of the heating takes place at the bottom right hand corner of the workload and that the temperatures reached at this point are about 100° C. In the center of the workload the temperatures have risen to only about 10° C.

The effect of moving the load towards the rear of the oven can be seen in Fig. 5. Again good agreement can be seen between the model and the experiments except, perhaps for the same overestimation of the corner effect. The position of the hot spot is now shown to be off center in both the model and the measurements.

Fig. 6 shows the calculated power dissipation in the workload. This information, which would be extremely difficult to derive from experiment, shows the temperature distribution profile which would be obtained if thermal effects such as conductivity, convection, and the variation in material properties with temperature were not taken into account. Comparison of these results with the actual temperature profiles show the importance of these effects in terms of a "smoothing" of the temperature distribution with respect to the power distribution. These effects would be more important if the heating time was longer.

XI. Implications for More Complex Scenarios

Although the test structure described here is comparatively simple, the same technique may be, and in fact has been, used for more complex loads such as "ready meals" with no increase in computer run time. Although studies have been made using idealized ready meals, e.g., [16], we are not aware of any model validations using such. Due to the variations within such products it is very difficult to get experimental results in a form which can be directly compared with the model. In these cases the model can be used to ascertain the effects of different changes in the geometry of the system in a controlled way regarding their relative capability for achieving a sufficiently uniform and rapid heating. This would be difficult experimentally.

XII. Conclusion

We have shown the feasibility of modeling the combined electromagnetic and thermal processes in a domestic microwave oven by means of the FDTD method implemented on just a moderately powered workstation and have shown comparisons with experimental results. Although the computer resources required are not trivial, (12 hours on an HP730 workstation being typical), the use of a model such as this to predict the effects of changes in the geometry of the oven and in the properties of the workload is still much quicker than building the necessary hardware for an experiment. The agreement obtained between prediction and experiment, while not perfect, is sufficient to show the main features of interest to the designer. Greater accuracy can, of course, be obtained by use of a finer mesh and more computer resources. Work is currently in progress into ways of speeding up the calculations by including analytical enhancements to the FDTD algorithm.

Acknowledgment

The authors from Bristol would like to thank Prof. J. McGeehan for the provision of facilities, and their colleagues in the Center for Communications Research for many helpful discussions.

References

[1] C. Flockhart, V. Trenkic, and C. Christopolous, "The simulation of coupled electromagnetic and thermal problems in microwave heating," in *Dig. 2nd Int. Conf. Computation in Electromagnetics,* Nottingham, Apr. 1994, pp. 267–270.

[2] D. Dibben and A. C. Metaxis, "Experimental verification of a finite element solution to heating problems in a multi-mode cavity," in *Proc. 2nd Int. Conf. Computation in Electroamagnetics,* Nottingham, Apr. 1994, pp. 135–137.

[3] Z. Shouzheng and J. B. Davies, "Non-linear modelling of microwave heating problems," in *Proc. 1st Int. Conf. Computation in Electromagnetics,* London, Nov. 1991, pp. 86–89.

[4] R. De Leo, G. Cerri, and V. Mariani, "TLM techniques in microwave ovens analysis: Numerical and experimental results," in *Proc. 1st Int. Conf. Computation in Electromagnetics,* London, Nov. 1991, pp. 361–364.

[5] W. B. Fu and A. C. Metaxis, "Numerical prediction of three-dimensional temperature distributions inside a microwave oven using the method of lines," *Dig. 2nd Int. Conf. Computation in Electromagnetics,* Nottingham, Apr. 1994, pp. 255–258.

[6] ——, "MAXEMOL—A numerical scheme for the solution of Maxwell's equations using the Method of Lines," in *Proc. Microwave and High Frequency,* Goteburg, Sweden, 1993, paper A5.

[7] C. K. Chou, G. W. Chen, A. W. Guy, and K. H. Luk, "Formulas for preparing phantom muscle tissue at various radio frequencies," *Bioelectromagnetics,* vol. 5, pp. 435–441, 1984.

[8] D. S. Engelder and C. R. Buffler, "Measuring dielectric properties of food products at microwave frequencies," *Microwave World,* vol. 12, no. 2, pp. 6–15, 1991.

[9] G. W. C. Kaye and T. H. Laby, "Tables of physical and chemical constants," 15th Ed., Longman, 1985.

[10] T. Ohlsson and P. O. Risman, "Temperature distribution of microwave heating—Spheres and cylinders," *J. Microwave Power,* vol. 13, no. 4, 1978.

[11] J. Mullin and J. Bows, "Temperature measurement during microwave cooking," *J. Food Additives and Contaminants,* vol. 10, no. 6, pp. 663–672, 1993.

[12] K. Yee, "Numerical solution of initial boundary value problems involving Maxwell's equations in isotropic media," *IEEE Trans. Antennas Propagat.,* vol. AP-14, pp. 302–307, 1966.

[13] J. Holman, Ed., *Heat Transfer,* 7th Ed. New York: McGraw-Hill, 1990.

[14] N. M. Pothecary and C.J. Railton, "A combined electromagnetic and thermal analysis of current sheet hyperthermia applicators," in *Proc. 24th EuMC,* Cannes, Sept. 1994.

[15] L. Barratt and D. Simons, "Experimental validation of a computer simulation of microwave heating," in *Proc. 27th Microwave Power Symp.,* Aug. 1992, pp. 118–122.

[16] J. R. Bows and P. S. Richardson, "Effect of component configuration and packaging material on microwave reheating a frozen three-component meal," *J. Food Science Technol.,* vol. 25, pp. 538–550, 1990.

Lizhuang Ma was born in Beijing, China. She received the Master's degree from the Department of Electronics Engineering, Tsinghua University in 1970 and the Ph.D. degree from Bath University in 1989.

From 1970 to 1984 she taught and pursued research in Department of Electronics Engineering, Tsinghua University. In the academic year 1984 and 1985 she was a Visiting Scholar at the School of Electrical Engineering, University of Bath, UK. Since 1992 she has been working in the Department of Electrical Engineering, University of Bristol as a Research Fellow. Her current interests include numerical techniques, mainly FDTD method, for modeling electromagnetic fields, and their applications in microwave heating and high speed computer system.

Dominique-Lynda Paul was born in Blida, Algeria, on January 16, 1961. She received the D.E.A. degree in electronics from Brest University in June 1986 and the Ph.D. degree from the "Ecole nationale Supérieure des Télécommunications de Bretagne" (LEST-ENSTBr) in January 1990.

Since then, she has been working as a Research Associate at the Communications Center, University of Bristol, where she has been involved in the modeling of passive planar microstrip circuits, in the characterization of dielectric devices at millimeter wavelengths and in the simulation of microwave heating systems.

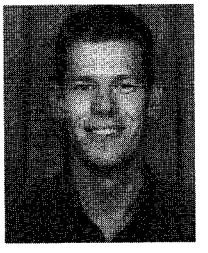

Nick Pothecary received the B.Eng. (Hons.) degree in electrical and electronic engineering from the University of Bristol in 1990 and the Ph.D. degree in Communications in 1994.

He is now working in the Center for Communications Research, University of Bristol and his current areas of research include radar and electromagnetic modeling for communication, industrial, and medical applications. He has also worked at the Ecole Nationale Supérieure des Télécommunications de Bretagne.

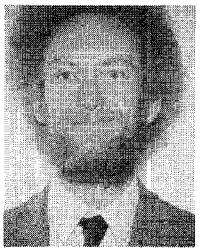

Chris Railton received the B.Sc. degree in physics with electronics from the University of London in 1974 and the Ph.D. degree in electronic engineering from the University of Bath in 1988.

From 1974 to 1984 he worked in the scientific civil service on a number of research and development projects in the areas of communications, signal processing, and EMC. Between 1984 and 1987 he worked at the University of Bath on the mathematical modeling of boxed microstrip circuits. He currently works in the Center for Communications Research at the University of Bristol where he leads the Computational Electromagnetics Group which is involved development of new algorithms and their application to MMICs, planar antennas, microwave and RF heating, EMC and high speed logic.

John Bows, photograph and biography not available at the time of publication.

Lawrence Barratt, photograph and biography not available at the time of publication.

Jim Mullin, photograph and biography not available at the time of publication.

David Simons, photograph and biography not available at the time of publication.